INTERNATIONAL JOURNAL OF TECHNOLOGY
ISSN: 2086-9614
http://www.ijtech.eng.ui.ac.id

CORRIGENDUM TO:

Cyclic Strain Rate Dependent Low-Cycle Fatigue Behavior of Alloy 617

Rando Tungga Dewa[1i], Aditia Aulia[1], Seon Jin Kim[2], Raja Akbar[1]

[1]*Department of Mechanical Engineering, Republic of Indonesia Defense University, IPSC Area Sentul, Bogor, West Java 16810, Indonesia*
[2]*Department of Mechanical Design Engineering, Pukyong National University, Busan 48547, Republic of Korea*

Raja Akbar's Affiliation type as Department of Mechanical Design Engineering, Pukyong National University, Busan 48547, Republic of Korea

Should be written as Department of Mechanical Engineering, Republic of Indonesia Defense University, IPSC Area Sentul, Bogor, West Java 16810, Indonesia

[i]Corresponding author's email: rando.dewa@idu.ac.id, Tel.: Tel.: +62 21-87951555; Fax: +62 21-29618761
doi: 10.14716/ijtech.v14i7.6658

International Journal of Technology 14(7) 1419-1427 (2023)
Received May 2023 / Revised September 2023 / Accepted November 2023

International Journal of Technology

http://ijtech.eng.ui.ac.id

Cyclic Strain Rate Dependent Low-Cycle Fatigue Behavior of Alloy 617

Rando Tungga Dewa[1*], Aditia Aulia[1], Seon-Jin Kim[2], Raja Akbar[2]

[1]*Department of Mechanical Engineering, Republic of Indonesia Defense University, IPSC Area Sentul, Bogor, West Java 16810, Indonesia*
[2]*Department of Mechanical Design Engineering, Pukyong National University, Busan 48547, Republic of Korea*

Abstract. Alloy 617 is identified as a potential material for defense applications, particularly in military air platforms. Therefore, this study aims to examine the impact of strain rate on Alloy 617 properties during low-cycle fatigue (LCF) at room temperature (RT). LCF life properties and damage mechanism of alloy 617 are examined across a strain rate range of ($5\times10^{-4} \sim 10^{-2}$ s^{-1}) in a fully-reversed controlled total strain range of 1.2%. Slow strain rate test (SSRT) is found to be a cost-effective method for assessing the material capability to respond to environmental interference. This study shows that LCF life of Alloy 617 is strongly influenced by the time-dependent mechanism, in terms of SSRT. The relationship between total strain, plastic strain, and time to failure with strain rates are established and expressed using the power law function to describe the fatigue life. Fractured specimens undergo metallography examination using an electron microscope, and fractography is discussed to differentiate the impact of SSRT on the physical damage characteristics under LCF loadings. LCF resistance of Alloy 617 is found to be time-dependent. Based on the results, it is recommended that the factor of safety must be considered in the designing phase to evaluate the fatigue life.

Keywords: Alloy 617; Fatigue life; Fractography; Low-cycle fatigue; Slow strain rate test

1. Introduction

In the strategy framework, advanced materials are identified as an important technology for driving innovation in defense. These materials represent a domain where the nation has globally competitive research and development capabilities for industrial strength as stated in the Indonesian National Strategy. The development of the new superalloy to be implemented for extreme conditions has attracted researchers and defense industries, specifically military air platforms. Among the emerging materials is Alloy 617, a solid solution-strengthened alloy composed of chromium, cobalt, and molybdenum, with added aluminum. This alloy is engineered to deliver a balance of heightened strength and stability at elevated temperatures. Additionally, it provides good properties for components of power generating plants, gas turbines, and high temperature superior required applications. Alloy is now being widely used for high-temperature applications (Dewa *et al.*, 2018a; Dewa *et al.*, 2018b; Dewa *et al.*, 2016; Ekaputra *et al.*, 2016; Redy *et al.*, 2010).

In the high-temperature environment, resistance to low-cycle fatigue (LCF) and creep-fatigue (CF) interaction is an important requirement for the successful design due to the

*Corresponding author's email: rando.dewa@idu.ac.id, Tel.: +62 21-87951555; Fax: +62 21-29618761
doi: 10.14716/ijtech.v14i7.6658

complex interactions between metals, high temperature, and air. LCF loadings are expected to result from thermally induced strain cycles and fluctuations during operations. Time-dependent mechanisms, influenced by environmental factors, have the potential to affect fatigue life synergistically or independently. Therefore, accurate prediction of LCF in extreme temperature conditions relies on characterizing a rate-controlling damage process that shapes cyclic deformation. This involves considering the appropriate combination of experimental stress/strain, temperature, strain rate, environment, and the prior metallurgical condition of the material (Sofyan *et al.,* 2010; Redy *et al.,* 2010). The effect of these time-dependent processes may reduce an alloy cyclic life resistance by orders of magnitude as compared to the room temperature (RT) behavior. Therefore, in this study, the phenomenon is initially tested on the laboratory scale to examine the damage mechanism, which is closely dependent on strain rate and the structures.

The literature on the slow strain rate deformation of alloy 617 is still rare, specifically at the initial RT setup. Recent studies show that the behavior observed in slow strain rate tests (SSRT) on stainless steel and structural steel is closely in line with the responses under creep conditions (Calmunger *et al.,* 2013; Luo *et al.,* 2013; Luo *et al.,* 2013). Numerous studies have been conducted to modify and improve the relationship to cover materials model through conventional or adapted methods (Ekaputra *et al.,* 2020; Suastika *et al.,* 2019; Chou *et al.,* 2016; Alie, 2016; Chen, Sun, and Chan, 2014; Nakai and Yokoyama, 2012). However, SSRT is found to be promising as a low-cost methodology for the evaluation of materials capability to respond to such environmental interference. The variance of strain rates in the order of magnitudes can be used in LCF test at RT. Understanding the variations in fractography appearance and applying accurate life prediction methods under these conditions provides crucial information for the ongoing rapid assessment of elevated temperature test behavior, specifically for Alloy 617.

The primary objective of this study is to determine the influence of individual and interactive time-dependent processes by performing SSRT under LCF loadings for Alloy 617 at RT. Furthermore, this finding focuses on the fatigue life interpolation methods, comparing their predictions to determine the suitability of the power-law relationship. The influence of change in strain rates on the damage mechanisms is also investigated. The aim is to establish a comprehensive understanding of LCF mechanism and draw conclusions related to the time-dependent damage.

2. Methods and Procedures

The composition (wt.%) of the commercial-grade Alloys used in this study is shown in Table 1. The as-received microstructure of the alloy 617 is shown in Figure 1, showcasing a fully austenitic face-centered cubic (FCC) structure known for maintaining superior mechanical properties at high temperatures (Dewa *et al.,* 2018a). Figure 2 shows the monotonic stress-strain behavior of Alloy 617, with FCC matrix, mainly consisting of nickel, cobalt, iron, chromium, and molybdenum. For microstructural analysis, the as-received sample was cross-sectioned and etched to reveal the grain structure. The sample was sequentially etched in solutions of hydrochloric acid, ethanol, and copper II chloride for at least 10-20 seconds. However, the microstructure appearance in Alloy 617 is well-uniformed equiaxed grains. The number of grains per unit was measured according to ASTM E112 to determine the average grain size. The small grain size ranges from 10 to 30 μm and the large grain size is approximately 40–100 μm in diameter.

For LCF tests, polished cylindrical specimens with a 6.0 mm diameter in the reduced section and a gauge length of 12.5 mm were used. The specimen design adhered to certain standards to prevent premature buckling or deformation under the highest tension stress anticipated during LCF test. Fully-reversed LCF tests were performed in ambient air at RT with different strain rates, i.e. $5x10^{-4}$, 10^{-3}, $6x10^{-3}$, and 10^{-2} s^{-1}, respectively, under 1.2% total strain range. A high-precision extensometer was attached to the specimen to record and collect the real-time data of the stress-strain response. Triangular waveforms were used for all LCF tests, with measurements of displacement, load, and strain signals taken for each cycle, comprising 200 data points. The test was concluded upon specimen separation or fracture, essential for a comprehensive examination of the complete fracture surface. However, the fatigue life criterion is defined according to the 25% reduction in stress range after the macrocrack is initiated. Finally, a metallography examination was carried out using Olympus GX51 Metallurgical Microscope and JEOL JSM Scanning Electron Microscope.

Table 1 Chemical composition of Alloy 617 (wt.%)

Ni	Cr	Co	Mo	Al	C	Fe	Ti	Si	Mn	Cu	P	S	B
53.11	22.2	12.3	9.5	1.06	0.08	0.949	0.4	0.084	0.029	0.027	0.003	<0.002	<0.002

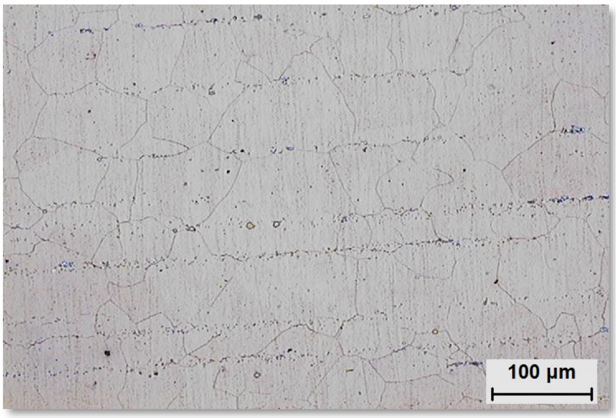

Figure 1 The as-received microstructure of Alloy 617

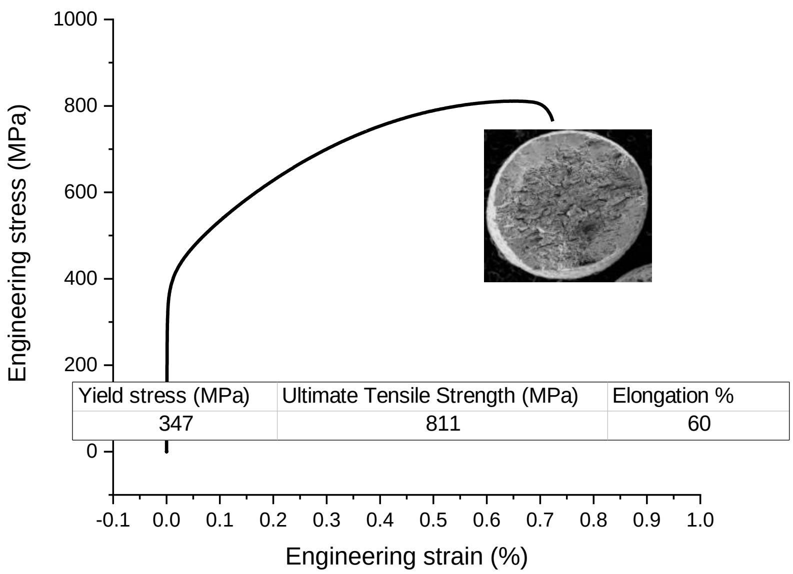

Figure 2 Monotonic stress-strain curve of Alloy 617

3. Results and Discussion

3.1. LCF life analysis

Figure 3 shows the influence of strain rate on LCF life indicating a decrease in fatigue life with lower strain rates. The linear relationship between fatigue life and strain rate can be drawn in the logarithmic function as shown in the Figure. The equation (1) used to describe the relationship is as follows:

$$\dot{\varepsilon} = A\left(N_f\right)^b \tag{1}$$

Where $\dot{\varepsilon}$ is strain rate, N_f is fatigue life in terms of the number of cycles to failure, and A and b are constants describing the regression fit (intercept and slope), respectively.

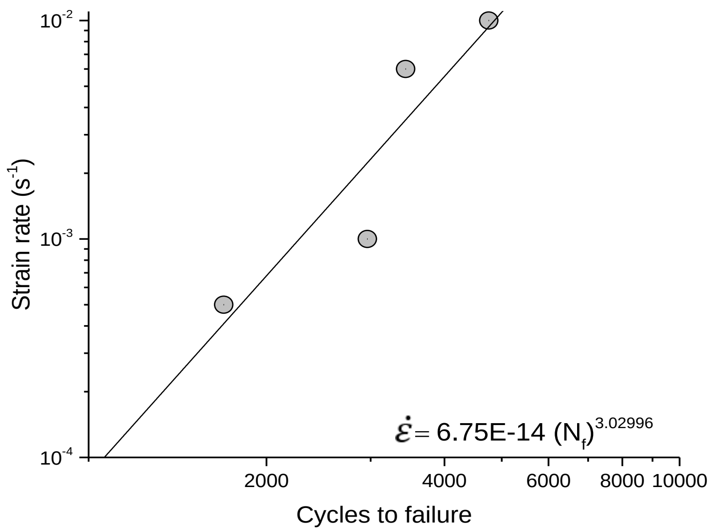

Figure 3 The function of LCF life with the variation of strain rates for Alloy 617

To provide a better understanding of the damage parameter, fatigue life function is then plotted in Figure 4, with plastic strain and time to failure spent until fracture. This relationship is described in the following equation (2):

$$\varepsilon_p = M(\dot{\varepsilon})^n \tag{2}$$

Where ε_p is strain rate, M and n are constants describing the regression fit (intercept and slope), respectively. The plastic strain values were derived from the mid-life of cycles to failure. It was assumed that the mid-life is best considered as the stabilized cycle for LCF testing at RT condition. According to Figure 4a, the lower strain rate test had a higher plastic strain. Furthermore, for LCF test with the influence of a time-dependent factor, the time to failure compared to that in terms of cycles to failure must be considered and can be shown in the following equation (3):

$$t_r = X(\dot{\varepsilon})^y \tag{3}$$

Where t_r is time to failure in terms of hour, X and y are constants describing the regression fit (intercept and slope), respectively. In Figure 4b, the time to failure with strain rates is plotted in a logarithmic function. Despite lower cycles to failure at lower strain rates, the time to failure exhibits a higher level. The equation generated from the time-to-failure function with strain rates for fitting interpolation is also provided in the Figure. The results show that the time-dependent crack mechanism is the dominant fatigue mechanism for Alloy 617 (Sah, Park, and Kim, 2023). The power law function seems to be well-fitted to the experimental data in terms of the linearity agreement, showing that the predicted life coincides well with the measured LCF life. This suggests that the time-dependent deformation can take place gradually with a slow strain rate fatigue (Luo *et al.,* 2013). In the verification process, the prediction techniques are confirmed with the predicted life derived by back-substituting experimental data into equations (Eq. 1 and 3). The estimated error accuracies are 12.6% and 13.7%, respectively. The results fall within a factor of 1.0 for conversion, affirming the observed linearity as shown in Figures. 3-4.

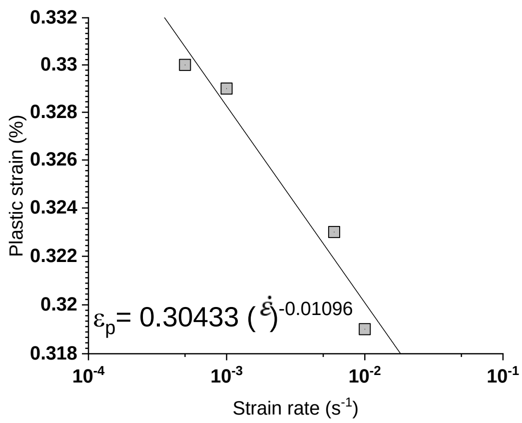

(a)

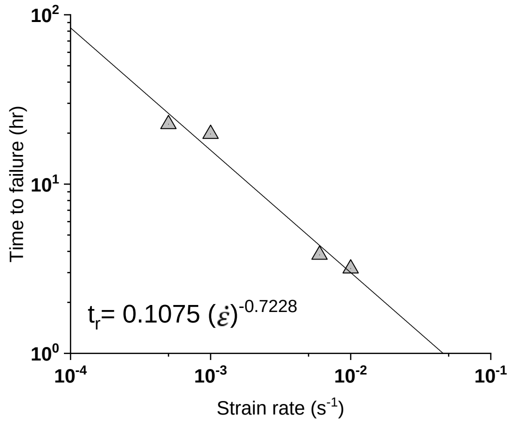

(b)

Figure 4 The plot of diagrams: (a) Plastic strain versus strain rates, and (b) Time to failure with strain rates function

3.2. Influence of strain rate on LCF properties

Cyclic stress response behaviors at different strain rates of Alloy 617 are shown in Figure 5. In Figure 5a, all materials show a similar trend with the initial hardening phase, followed by cyclic softening and rapid drop of stress or failure. This is typical cyclic stress response behavior of superalloy under LCF loading at RT. Based on the result, a significantly lower strain rate test condition decreases the strength of the material, which can be seen in the lower stress range response (pink dot line). Furthermore, Figure 5b shows cyclic stress responses in order of normalized cycle. The materials show a short initial hardening of about 5% of the fatigue life. The initial hardening occurred due to the increasing dislocation density of fatigue slips in material reconciliation. The increase in the number of cycles leads to an augmentation in dislocation movement. When the rate of dislocation multiplication equals the rate of dislocation annihilation, cyclic stress becomes stabilized (Ekaputra *et al.,* 2016). Accordingly, the material shows significant cyclic softening gradually (almost for the entire life) until the initiation of macrocrack where the stress suddenly dropped. Cyclic softening phase of this material may be due to the annihilation of dislocations that exceed the dislocation multiplication, therefore, cyclic stress is decreased. Subsequently, at lower strain rates, there is a decrease in dislocation mobility, consequently leading to a reduced stress range (Sah, Hwang, and Kim, 2021). From the Figure, it can also be observed that the macrocrack initiation for the specimen with the fastest strain rate occurred earlier. Cyclic crack propagation is much higher for a high strain rate specimen.

To quantify the degree of cyclic softening during LCF, the softening ratio is defined as the ratio between the peak stress after initial hardening (S_{max}) and the stress at the sudden drop point (S_c). Figure 6 shows the degree of softening phase at different strain rates. It can be seen from the Figure that the trend of degree of softening increases generally with an increase in strain rate. The impact of cyclic softening phase is more pronounced at higher strain rates. This is attributed to the higher number of cycles to failure and accumulated plastic deformation compared to specimens tested at lower strain rates. This result is in line with the earlier discovery that at higher strain rates, there is an increase in dislocation mobility, leading to a heightened stress response, and vice versa (Nakai and Yokoyama, 2012).

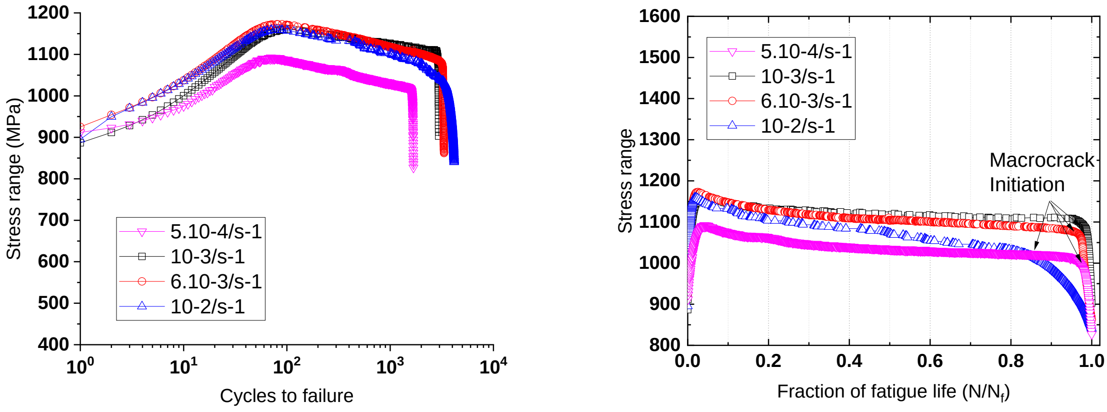

(a) (b)

Figure 5 (a) Cyclic stress response behavior at different strain rates of Alloy 617, and (b) Normalised cycle of cyclic stress response curves

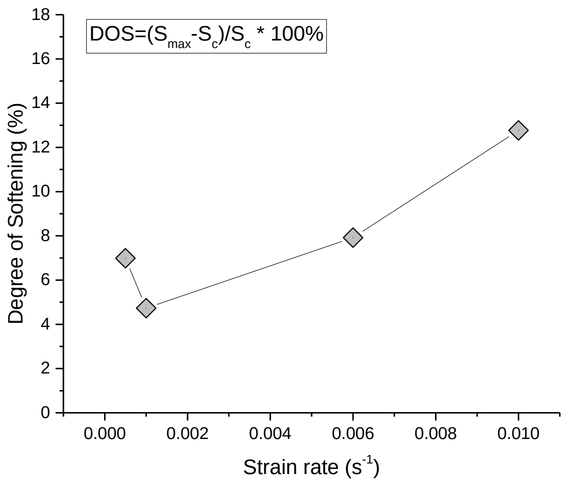

Figure 6 Degree of softening ratio at different strain rates of Alloy 617

3.3. Fractography examination

Figure 7 shows typical fractography SEM micrographs (with zoomed images on each zone) for LCF specimens tested at a high strain rate. Figure 7c shows a typical fatigue fracture consisting of the initiation zone (pointed by the black arrows), Figure 7b shows the crack propagation area, and Figure 7a shows the final fracture zone in the dashed line. In the crack initiation zone, the fracture surface shows cleavage-like facets. The crack propagation predominantly shows a flat surface characterized by dense striations and a limited number of secondary cracks. The sharp features on the surface, indicative of substantial tension during fracture, contribute only a small portion to the final fracture zone. However, the failure modes generally show a transgranular crack in nature with cleavage-like facets for typical fatigue loadings at RT. This type of crack shows that fatigue failure occurred due to the slips at the surface. No indications of premature failure or defect failure are noticed during the examination. Furthermore, Figure 8 shows SEM micrographs (with zoomed images on each zone) for LCF specimens tested at a low strain rate. For low strain rate specimens, however, the crack propagation can be characterized into two stages (separated by a yellow line). The first stage in Figure 8c shows a typical transgranular fracture with a bigger step of striations, and it is related to the lower cycle. Subsequently, the second stage in Figure 8b shows the domination of secondary cracks. It is hypothesized that the occurrence of secondary cracks precedes the arrival of the main crack tip. These secondary cracks can be originated from typical cavities/voids. At the final fracture zone, intergranular dimple fracture is even more obvious. The failure mode shows an intergranular fracture mechanism with creep (Sah, Hwang, and Kim, 2021). Therefore, it can be shown that the intergranular crack-fatigue interaction can be promoted at a very low strain rate LCF loading even at RT, as the deformation of grain boundary sliding is more prevalent at this condition and results in lower cycles to failure. Therefore, a lower fatigue life at a very low strain rate can be expected from this mechanism during fatigue. The findings shows that a longer tensile loading rate per cycle is needed for the type of experiment which increases this cavities-driven crack interaction. The results are substantiated under lower strain rate conditions, where the strength is reduced, accompanied by higher ductility and a slower softening rate. Consequently, the dislocation mobility is constrained in comparison to specimens tested at high strain rates (Sah, Hwang, and Kim, 2021; Redy *et al.,* 2010). Additionally, valuable observations obtained from the continuous rapid assessment of the environmental test behavior for the studied material, given the significant connection to time-dependent behavior, are crucial for further understanding.

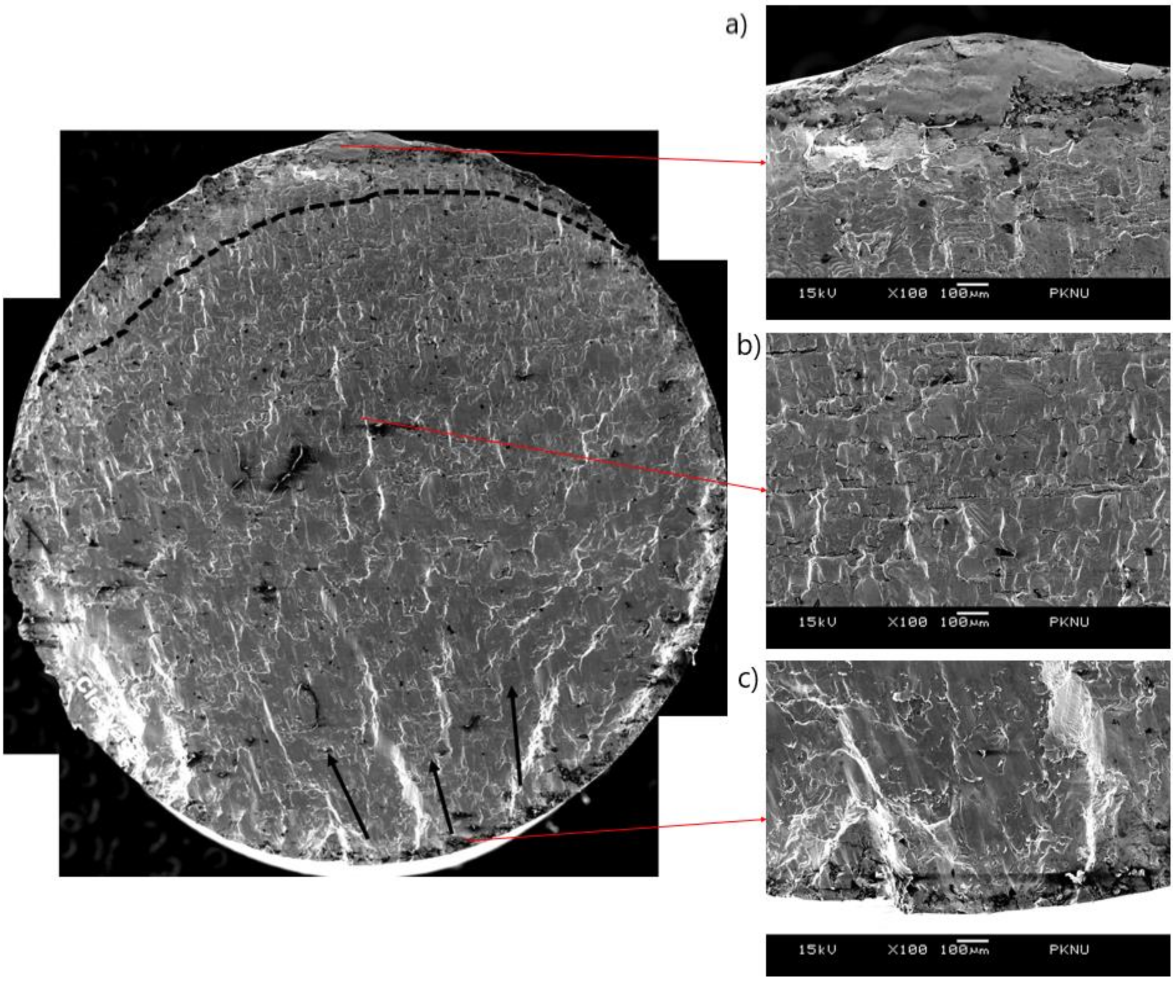

Figure 7 SEM micrographs of fracture surface specimen tested at 10^{-2} s-1, showing typical: (a) Failure zone features, (b) Crack propagation, and (c) Crack initiation

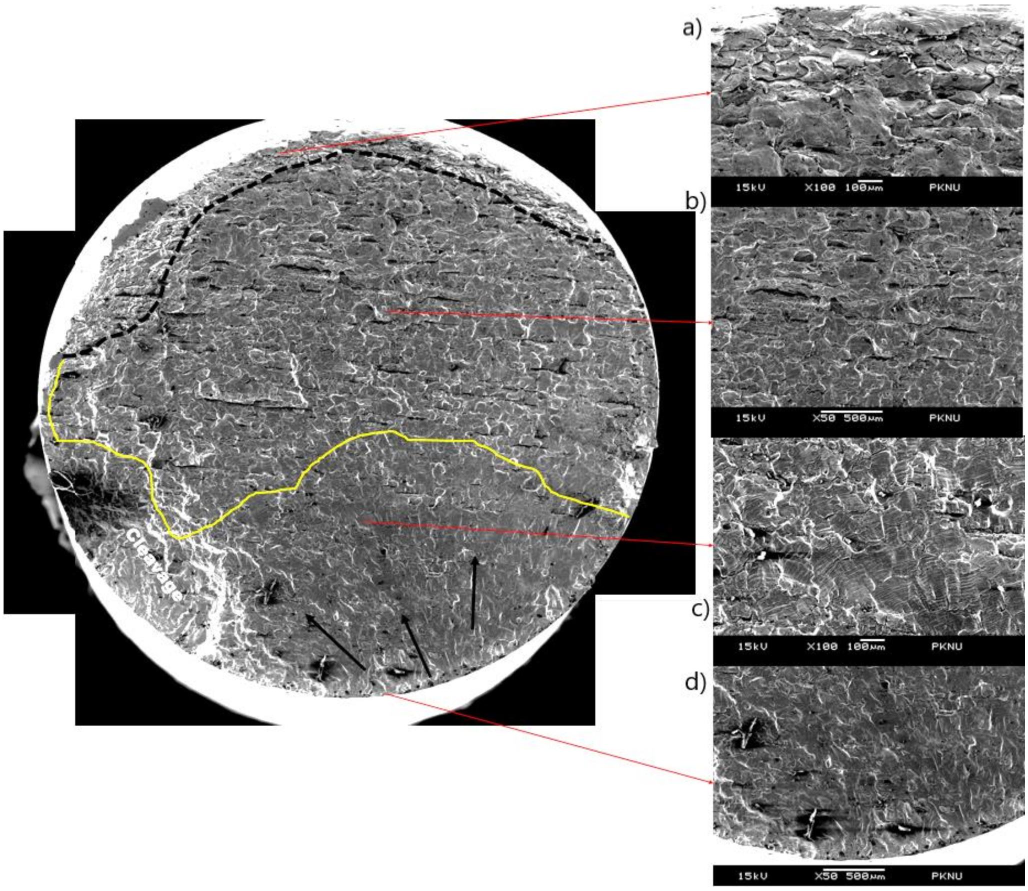

Figure 8 SEM micrographs of fracture surface specimen tested at $5x10^{-4}$ s-1, showing typical: (a) Failure zone features, (b) Second stage of crack propagation, (c) First stage of crack propagation, and (d) Crack initiation

4. Conclusions

In conclusion, LCF resistance of Alloy 617 was found to be time-dependent over a range of $5x10^{-4} \sim 10^{-2}$ s^{-1} strain rates. All materials showed a similar trend with an initial hardening phase, followed by cyclic softening and a rapid drop of stress or failure. However, it was observed at a lower strain rate that the specimen had a lower stress range compared to other specimens and the macrocrack initiation for specimen with the fastest strain rate occurred earlier. The influence of strain rates on fatigue life was evidenced through fractography images. At the lowest strain rate, the specimen fractured with additional failure mode in an intergranular manner. The domination of secondary cracks was obvious at the surface, possibly originating from cavities or voids. A typical mixed intergranular dimple fracture for the very low strain rate specimen similarly indicated the interaction of cavities-driven cracking mechanism during fatigue loading at RT, attributing to the lower LCF life. It was recommended that the factor of safety should be considered in the designing phase to evaluate the fatigue life. The fatigue life variation could be extremely broad at millions of cycles, specifically out of time-dependent damage towards catastrophic failure.

Acknowledgments

The authors express gratitude and acknowledge the mutual collaboration between universities. The dissemination of this study was funded by the Republic of Indonesia Defense University and the research was carried out at Pukyong National University.

References

Alie, M.Z.M., 2016. The Effect of Symmetrical and Asymmetrical Configuration Shapes on Buckling and Fatigue Strength Analysis of Fixed Offshore Platforms. *International Journal of Technology*. Volume 7(6), pp. 1107-1116

Calmunger, M., Chai, G.C., Johansson, S., Moverare, J., 2013. Damage and Fracture Behaviours in Aged Austenitic Materials During High-Temperature Slow Strain Rate Testing. *Key Engineering Materials,* Volume 592–593, pp. 590–593

Chen, Y., Sun, W., Chan, T.-M., 2014. Cyclic Stress-Strain Behavior of Structural Steel with Yield Strength Up To 460 N/mm^2. *Frontiers of Structural and Civil Engineering*, Volume 8(2), pp. 178–186

Chou, L.H., Chiou, Y.C., Wu, C.C., Huang, Y.J., 2016. Predictions of the Stress-Strain Curve and Fatigue Life for AISI 316 Stainless Steel in Cyclic Straining. *Journal of Marine Science and Technology*, Volume 24(3), pp. 426-433

Dewa, R.T., Kim, S.-J., Kim, W.-G., Kim, E.-S., 2016. Understanding low cycle fatigue behavior of alloy 617 base metal and weldments at 900 °C. *Metals*, Volume 6(8), p. 178

Dewa, R.T., Kim, S.-J., Kim, W.-G., Kim, E.-S., 2018b. Evaluation of the low cycle fatigue failure properties for GTAW weldments of alloy 617 at 950 °C. *Engineering Failure Analysis*, Volume 90, pp. 202–214

Dewa, R.T., Park, J.-H., Kim, S.-J., Lee, S.-G., 2018a. High-temperature creep-fatigue behavior of alloy 617. *Metals*, Volume 8, p. 103

Ekaputra, I.M.W, Dewa, R.T., Haryadi, G.D., Kim, S.J., 2020. Fatigue Strength Analysis of S34MNV Steel by Accelerated Staircase Test. *Open Engineering*, Volume 10(1), pp. 394–400

Ekaputra, I.M.W., Kim, W.-G., Park, J.-Y., Kim, S.-J., Kim, E.-S., 2016. Influence of Dynamic Strain Aging on Tensile Deformation Behavior of Alloy 617. *Nuclear Engineering and Technology*, Volume 48, pp. 1387–1395

Luo, Y., Huang, C., Guo, Y., Wang, Q., 2012. Energy-Based Prediction of Low Cycle Fatigue Life of High-Strength Structural Steel. *Journal of Iron and Steel Research International,* Volume 19(10), pp. 47–53

Luo, Y., Huang, C., Tian, R., Wang, Q., 2013. Effects of Strain Rate on Low Cycle Fatigue Behaviors of High-Strength Structural Steel. *Journal of Iron and Steel Research International,* Volume 20(7), pp. 50–56

Nakai, K., Yokoyama, T., 2012. High Strain-Rate Compressive Properties and Constitutive Modeling of Selected Polymers. *Journal of Solid Mechanics and Materials Engineering*, Volume 6(6), pp. 731–741

Redy, G.V.P., Harini, P., Sandhaya, R., Rao, K.B., Paretkar, R.K., 2010. On dual-slope linear cyclic hardening of Hastelloy X. *Materials Science and Engineering A*, Volume 527, pp. 3848–3851

Sah, I.J., Hwang, J.B., Kim, E.S., 2021. Creep Behavior of Diffusion-Welded Alloy 617. *Nuclear Engineering and Technology*, Volume 329, pp. 142–146

Sah, I.J., Park, J.H., Kim, E.S., 2023. Fatigue Life Curves of Alloy 617 In the Temperature Range of 800–950 °C. *Nuclear Engineering and Technology*, Volume 55(2), pp. 546–554

Sofyan, B.T., Berndt, C.C., Stefano, M., Pardede, H.J., 2010. WC-Co Coatings for High-Temperature Rocket Nozzle Applications: An Applications Note. *International Journal of Technology*. Volume 1(1), pp. 48–56

Suastika, K., Sahlan, S., Nugroho, W.H., Zubaydi, A., Misbah, M.N., Murdjito, M., 2019. Fatigue Life Assessment of Waste Steel Reused as Tsunami Buoy Keel Structures: A Case Study. *International Journal of Technology*, Volume 10(4), pp. 700–709